

Copyright © 2007 IEEE. Reprinted from IEEE TRANSACTIONS ON NUCLEAR SCIENCE

This material is posted here with permission of the IEEE. Such permission of the IEEE does not in any way imply IEEE endorsement of any of Jet Propulsion Laboratory's products or services. Internal or personal use of this material is permitted. However, permission to reprint/republish this material for advertising or promotional purposes or for creating new collective works for resale or redistribution must be obtained from the IEEE by writing to pubs-permissions@ieee.org.

By choosing to view this document, you agree to all provisions of the copyright laws protecting it.

Radiation Response of Emerging High Gain, Low Noise Detectors

Heidi N. Becker, William H. Farr, and David Q. Zhu

Abstract—Data illustrating the radiation response of emerging high gain, low noise detectors are presented. Ionizing dose testing of silicon internal discrete avalanche photodiodes, and 51-MeV proton testing of InGaAs/InAlAs avalanche photodiodes operated in Geiger mode are discussed.

Index Terms—Avalanche photodiode, excess noise factor, internal discrete avalanche photodiode, photon counting.

I. INTRODUCTION

SEVERAL novel technologies are being explored by NASA for use in photon counting applications. Although classic avalanche photodiodes (APDs) provide higher internal gain and can achieve better signal to noise performance than many other semiconductor detectors (e.g., p-n or p-i-n junction photodiodes in certain applications [1]), they still suffer from a relatively high excess noise factor when operated at very high gain. This limits their potential in applications such as interplanetary optical communications, where photon counting at very high gain will be required. The near term focus is ground-based optical communications receivers, but it is expected that the field will naturally progress toward space-born receivers in Earth or Mars orbit. One benefit would be the lack of atmospheric interference. LIDAR applications represent an additional forum for detectors with high detection efficiency. The goal of this study was to begin to understand how space radiation effects will alter the operational performance of candidate technologies prior to the end of their development phase.

Engineering samples for two technologies were studied: (1) Silicon Internal Discrete Avalanche “IDA” Photodiodes (a.k.a. Discrete Amplification Detectors “DADs”) by Amplification Technologies, Inc., and (2) InGaAs/InAlAs APDs (operated in Geiger mode) by Spectrolab. Descriptions of each technology, including their advantages over classic APDs, are provided below. This preliminary testing focused on the likely *dominant* area of vulnerability for each technology, based on historical precedent and best engineering judgment, given a general understanding of the design. Irradiation levels were chosen based on expected radiation environments for applications in Earth or Mars orbit. Devices were characterized before and after irradiation in JPL’s Optical Communications Detector and Receiver Calibration Facility.

Manuscript received September 20, 2006; revised January 12, 2007. This work was carried out at the Jet Propulsion Laboratory, California Institute of Technology, under a contract with the National Aeronautics and Space Administration as part of the NASA Electronic Parts and Packaging Program, Code Q.

The authors are with the Jet Propulsion Laboratory, California Institute of Technology, Pasadena, CA 91109 USA (e-mail: Heidi.N.Becker@jpl.nasa.gov; William.H.Farr@jpl.nasa.gov; David.Q.Zhu@jpl.nasa.gov).

Digital Object Identifier 10.1109/TNS.2007.894179

II. SILICON IDA PHOTODIODES

A. Description of IDA Mechanism

The excess noise factor (F) is a parameter which quantifies the amplification noise of a detector. It is related to the statistics of gain (M) as follows:

$$F = \frac{\overline{M^2}}{\overline{M}^2} = 1 + \frac{\sigma^2}{\overline{M}^2} \quad (F = 1 \text{ for an ideal amplifier}) \quad (1)$$

where σ^2 is the variance of the gain. The McIntyre gain probability distribution of classic APDs is relatively broad [2], [3], particularly at high gains. This leads to typical excess noise factors of 2 or more in silicon APDs at gains of only a few hundred [4]. Although IDA technology uses the same avalanche multiplication process to achieve gains as high as 100,000, its design allows it to overcome the stochastic nature of this amplification mechanism. In IDA devices, the input signal is separated into multiple *spatially separate* channels, each channel containing the same number of elementary charges. The size of the incoming signal determines how many of the individual channels are utilized. The packet of elementary charges in each channel is multiplied by the same amplification factor, causing a calibration of the amplified signal packets that are read out from the detector. The avalanche multiplication responsible for this amplification is internally controlled by space charge screening to ensure that each signal packet reaches essentially the same gain. This leads to a very narrow gain distribution and thus a correspondingly low excess noise factor.

One implementation of a discrete amplifier [5] is an array of channels, each one containing a silicon p-n junction. Each of these junctions is coupled to an n+ polysilicon conductive channel electrode. The array of channel electrodes is separated from a common “readout” electrode by an insulator layer which capacitively couples the channel electrodes to the common. The channel electrodes are also coupled to the common by a wide band gap semiconductor plug (such as SiC). Fig. 1 shows a conceptual sketch of an IDA channel, adapted from [5].

The supply voltage is set such that the potential across the avalanche region is slightly larger than the breakdown value. Avalanche multiplication causes electrons to accumulate on the channel electrode, until the field is such that multiplication ends via “negative feedback” (the accumulated charge screens the field). Because the channel electrodes and the common are capacitively coupled, an “image” charge builds up on the common electrode. The build up of amplified signal charge on the channel electrode begins a process where the potentials in the various regions of each channel change. This leads to a switching mechanism that allows the readout of the amplified signal and simulta-

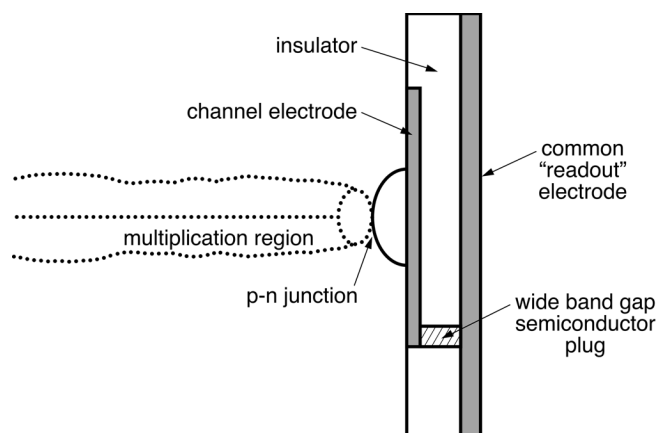


Fig. 1. Conceptual sketch of a single IDA channel (adapted from U.S. Patent 6,885,827).

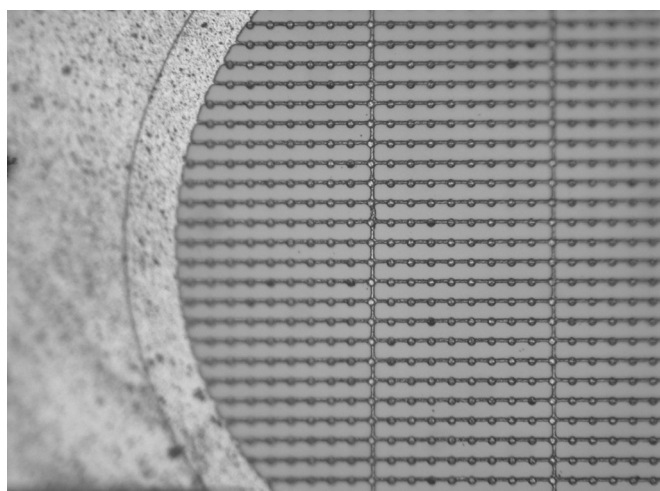


Fig. 2. Optical microscope image of the top surface of an IDA test sample. It is an array of many channels.

neously leads to the reset of the channel to its original state—a high potential across the avalanche region.

Fig. 2 is an optical microscope image of the top surface of an IDA test sample. The image illustrates that the detector active area is an array of many channels. The tested samples incorporate cellular Si/SiO₂ interfaces under aluminum contact regions. Focused ion beam (FIB) etching and electron dispersive spectroscopic (EDS) scanning electron microscopy (SEM) analysis were performed on one of the samples. Fig. 3 is a SEM image of an etched region. Elemental analysis confirmed the presence of an oxide layer between the aluminum electrode region and the “floating” mesa regions to either side of the center contact. The mesa regions have a high silicon content and may be polysilicon channel electrodes for two adjacent channels.

B. IDA Experimental Methods

Because of the dependence of the IDA switching mechanism on various potentials within the amplification channels (and the importance of the oxide layer that capacitively couples individual channel electrodes to the readout electrode), it was decided to focus the radiation testing effort on the impact of ion-

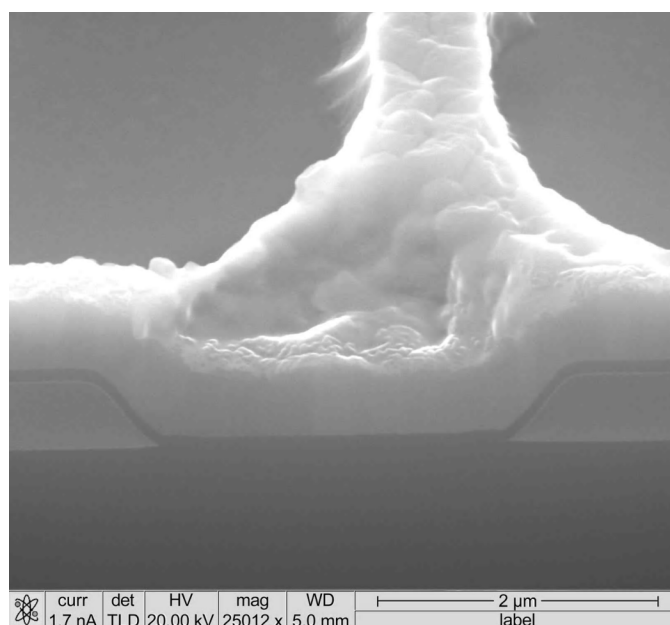


Fig. 3. SEM image of a FIB-etched IDA sample. The two floating “mesa” regions are separated from the aluminum contact by an oxide layer. The mesas may possibly be polysilicon channel electrodes for two adjacent channels.

ization damage. Total ionizing dose (TID) irradiations were performed at JPL’s Co-60 gamma facility, using a 50 rad(Si)/s dose rate. IDA samples were irradiated at ambient temperature while under static bias. The bias condition was chosen based on the voltage that yielded the best performance prior to irradiation, but was adjusted down by several volts in an effort to protect the samples from experiencing an extended breakdown mode from radiation-induced shifts during the irradiation period (the optimal voltage for pre-irradiation performance is very near to the breakdown voltage). The first post-irradiation characterizations were performed less than 2 hours after irradiation.

Characterizations were performed with the samples at 295 K in a light-tight dewar. 850 nm light was fed into the dewar through a fiber optic cable, and was collimated before illuminating the active region. The IDA output was processed using software which determined pulse amplitude and count rate statistics. Dark count rates, count rates under 850 nm illumination, the mean and standard deviation of the pulse amplitudes, and pulse-width statistics were examined. The excess noise factor was determined pre- and post-irradiation.

C. Results of IDA Ionizing Dose Testing

This paper focuses on the engineering unit with the best pre-irradiation performance (“2M”). Prior to irradiation, the optimal operational mode (at 295 K) was found when a supply voltage of 80V was applied (a voltage of 73 V was applied during irradiation). Under these conditions, the count rate under illumination was 2.1×10^7 cps, the dark count rate was 4×10^4 cps, and the pulse widths were narrow (<1 ns). The mean pulse amplitude was 80 mV (50 Ohm, 500X amplification, 1 GHz BW) with a standard deviation of 24 mV. Applying (1), these pulse amplitude statistics yield an excess noise factor of 1.09. Fig. 4 shows an oscilloscope frame that was saved during pre-irradiation illumination with 850 nm photons. The pulse amplitude uniformity

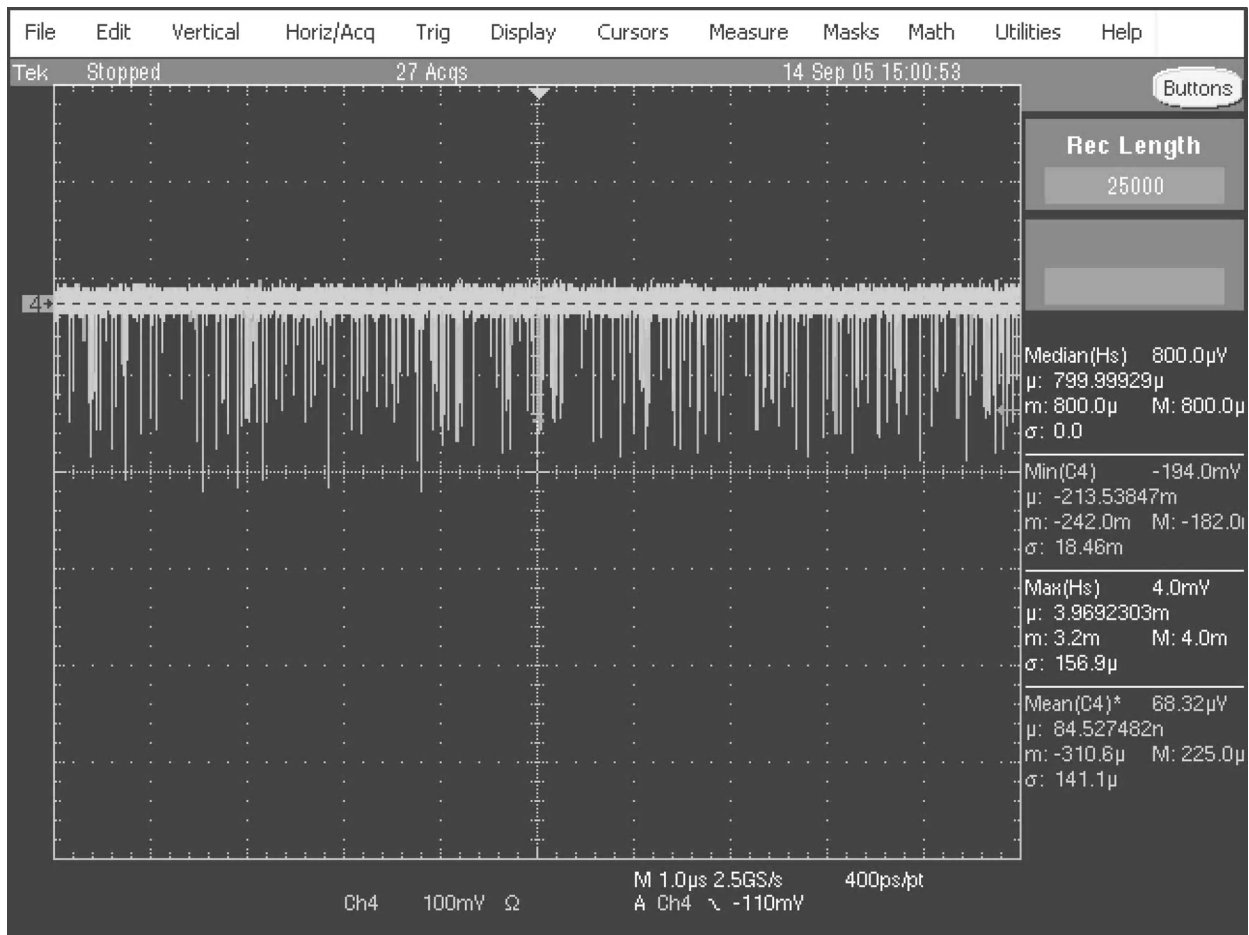


Fig. 4. Pulses observed during illumination of IDA sample “2M” with 850 nm photons. Data was taken prior to irradiation at 295 K using an 80 V supply voltage. The vertical scale division is 100 mV. The mean pulse amplitude (using 50 Ohm, 500X amplification, and a 1 GHz bandwidth) was 80 mV, with a standard deviation of 24 mV. This yields an excess noise factor of 1.09.

(in the negative-going signals), which results in such a low excess noise factor in this technology, can be seen.

Following irradiation to 5 krad(Si), a significant mode shift was observed at the operational conditions used for the pre-irradiation characterization. Inverted (positive) pulses and a general broadening of the pulse width were observed (see Fig. 5). The pulse amplitude statistics were corrupted by the presence of many inverted (positive) pulses. The dark count rate decreased to 477 cps, and the count rate under illumination decreased by two orders of magnitude. Although the counting efficiency experienced a large decrease after 5 krad(Si), the irradiation *did not increase the excess noise factor* nor did it dramatically change the average pulse amplitude.

The sample was characterized again 6 hours, 24 hours, and 1 month after the first post-irradiation characterization (between measurements, the sample was stored unbiased at room temperature). Table I shows the observed changes in performance parameters following irradiation and after the 1 month annealing period. The three data sets shown at the 5 krad(Si) level were taken less than 2 hours after the irradiation. These data were collected in rapid succession, following adjustment of the supply voltage to 79, 78.6, and 78.1 V, respectively. Although inverted pulses were not observed at 78.6 and 78.1 V, the count rates were quite poor compared to those seen at 79V. The observed

trend over the 1 month annealing period was a gradual decrease in the supply voltage required to put the sample into the broad inverted pulse mode, and the counting efficiency did not regain its pre-irradiation level under any bias condition.

We suspect that radiation-induced trapped charge in the dielectric bulk, or traps at the SiO_2/Si interfaces in each channel, may screen the field in the amplification regions such that a larger number of accumulated carriers is required at the channel electrode to quench the amplification process. This may occur over a significantly longer period of time than in an un-irradiated sample, and may even require multiple channel inputs before amplification finally ceases. This could be the cause of the reduced count rates seen after irradiation. A relatively thick oxide (~ 100 nanometers) is used between the aluminum contact and the floating mesa regions described in Section II.A, so the trapped charge could be significant. The broadened pulse widths that were observed after the irradiation indicate that the potentials within each channel that control the switching/readout mechanism are also impacted by ionizing dose.

It is interesting that the excess noise factor remains low following irradiation (although the count rate is greatly decreased). This is probably because the amount of signal amplification that occurs before readout is a function of the capacitance of the insulator layer between the channel electrodes and the common.

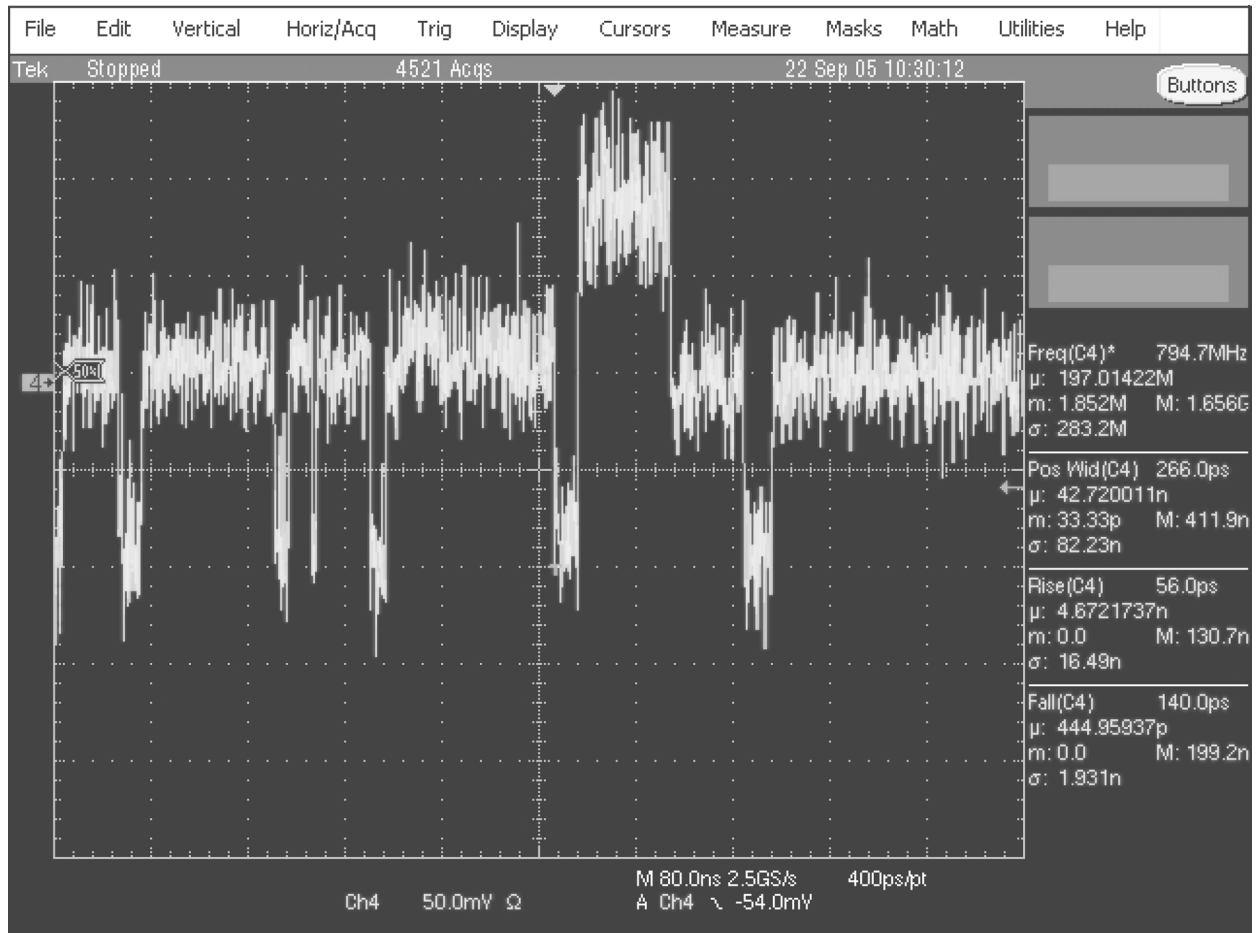


Fig. 5. Pulses following irradiation to 5 krad(Si). The same operational conditions were used as in Fig. 4. In this oscilloscope frame the vertical scale division is 50 mV.

Ionizing dose does not appear to be affecting the capacitance, since similar pulse amplitudes were observed before and after the irradiation.

We were surprised by the continued decrease in the supply voltage required to induce the broad, inverted pulse mode over the 1 month annealing period. However, it is likely that any migration of charge during this period was very subtle. If we compare dark IV curves for 2M taken at the various steps in the experiment (Fig. 6), we see that the “knee” became much sharper following irradiation. This knee drifted down and to the left (towards lower biases) with time. This is consistent with a breakdown mode occurring at lower supply voltages over time. However, note that the decreases in dark current at voltages below breakdown were rather small.

III. InGaAs/InAlAs APDs

A. Description of InGaAs/InAlAs APD Technology

InGaAs/InAlAs APDs use an *InAlAs avalanche layer* in place of the InP avalanche layer that is used in conventional InGaAs/InP APDs. Both technologies have an InGaAs absorption layer, but in InGaAs/InAlAs APDs, the absorption layer is *not depleted* and no impact ionization occurs within it [6]. The undepleted absorption layer and InGaAs/InAlAs material system yield a lower dark current, and a lower excess

noise factor, than InGaAs/InP APDs. Lower excess noise (a narrow pulse amplitude distribution) allows the use of a lower discriminator threshold for rejecting dark counts; this increases photon counting efficiency [7].

B. InGaAs/InAlAs APD Experimental Methods

Because of their structural similarity to InP/InGaAs APDs, it was decided to focus the radiation testing effort on displacement damage dose (DDD) effects. Previously, comparative proton and Co-60 gamma testing of InP/InGaAs APDs [8] has shown displacement damage to be the dominant contributor to device degradation, particularly affecting dark current. 51-MeV proton irradiations were performed on two samples at ambient temperature with all leads grounded. Sample “#1” was irradiated to 6.25×10^{10} p/cm² and returned to JPL’s cryogenic test bed for characterization. A second irradiation was performed one month later to bring the cumulative fluence to 1.25×10^{11} p/cm². Sample “#2” was irradiated to 3.1×10^{10} p/cm².

Characterizations were performed in a light-tight dewar at temperatures ranging from 100–297 K. IV curves were taken in the dark and under 1064 and 1534 nm illumination. Counts per second were recorded under several flux levels of 1064 nm and 1534 nm photons. An active quenching circuit was used to apply 5-ns 2.5 V pulses on top of the dc supply voltage, with a 100 kHz

TABLE I
PERFORMANCE PARAMETERS FOR IDA SAMPLE 2M

Radiation Level	Vs above which inverted pulses were observed (V)	Optimal supply voltage [non-inverted pulses] (V)	Dark count rate (cps)	Count rate (cps)	Excess Noise Factor	Pulse Width (ns)	Mean pulse amplitude [50 Ohm, 500X amplification, 1GHz BW] (mV)
0 krad(Si) Pre-radiation	-	80-82	$\sim 4 \times 10^4$	$2.1 \times 10^7 - 3.4 \times 10^7$	1.09-1.10	<1	80-100
5 krad(Si)	79	79	477	1.5×10^5	1.08	11(avg) 32(σ)	117
		78.6	60	8.9×10^3	1.06	<1	56
		78.1	0	0	-	-	-
5 krad(Si) + 24 hr anneal	78	76.2	0	1.3×10^5	1.01	26 (avg)	138
5 krad(Si) + 1 mo anneal	76	75.4	0	2.8×10^6	1.04	18 (avg)	91

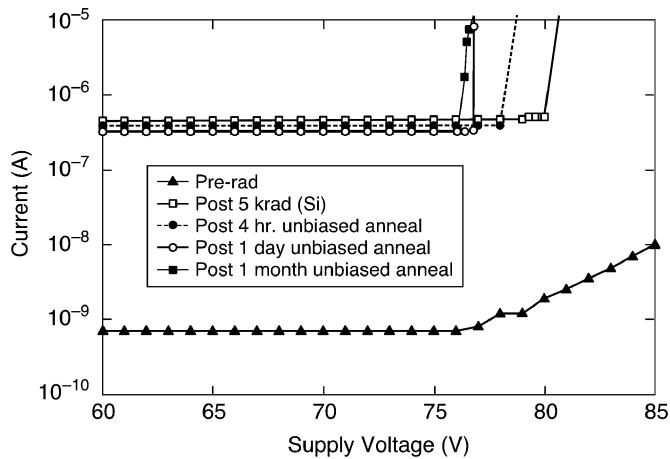


Fig. 6. Dark IV curves for 2M at various steps in the experiment. The “Post 5 krad (Si)” data was collected less than 2 hours after the end of the irradiation.

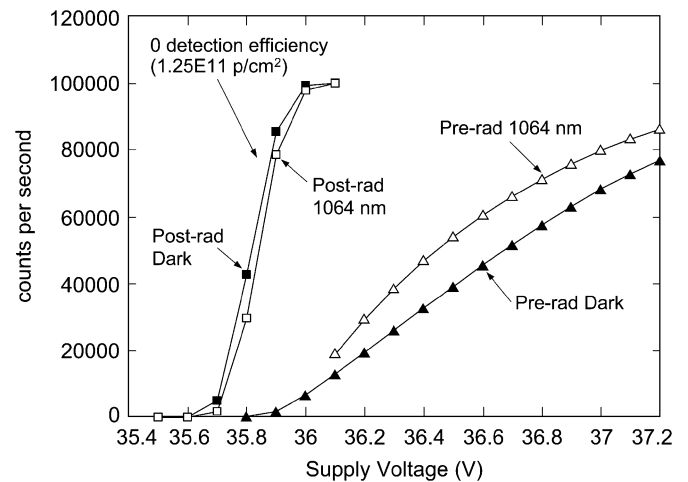


Fig. 7. Pre- and post-irradiation count rates for Spectrolab sample #1 at 200 K. The maximum pre-irradiation detection efficiency was 4.1% at 36.5 V.

rep rate. At supply voltages close to the knee in the detector’s IV curve, the extra potential provided by these pulses is enough to put the detector into Geiger mode (V_s > than breakdown voltage) for 5-ns periods. While in Geiger mode, the avalanche multiplication is extreme, gain is very high, and the detector is able to count photons. Count rates were recorded while the detector under test was illuminated in the pulsed Geiger mode.

C. Results of InGaAs/InAlAs APD Proton Testing

Reduced photon count rates were observed following the proton irradiations. For sample #1, after fluences of 6.25×10^{10} p/cm² and 1.25×10^{11} p/cm², the count rates under 1064 nm and 1534 nm illumination were dominated by the corresponding dark count rates. This was the case over the full temperature range used for the characterizations (100 K to 297 K). For example, at 100 K, the maximum detection efficiency of Spectrolab sample #1 under 1064 nm photon illumination had been 9.1% (at 33.7 V) prior to irradiation. It dropped to less than 2%

(at 34.6 V) after a fluence of 6.25×10^{10} p/cm², and to 0.8% (at 34.2 V) after a fluence of 1.25×10^{11} p/cm².

Fig. 7 shows count rates for sample #1 at 200 K. Dark count rates and count rates under 1064 nm photon illumination are compared for pre- and post-irradiation (1.25×10^{11} p/cm²) conditions. At this irradiation level, the detection efficiency was zero at 200 K. There is a dramatic increase in the dark count rate following this fluence, and the count rate under illumination is actually slightly lower. It is not presently understood why the rates under illumination would be less, but a similar effect has been observed in un-irradiated devices when comparing dark current to photocurrent at low supply currents [7]. Prior to irradiation, the maximum detection efficiency had been 4.1% (achieved at a supply voltage of 36.5 V).

Fig. 8 shows IV curves for sample #1 at 200 K. Prior to irradiation, the dark IV curve had a fairly distinct “knee” near the breakdown voltage of the device. Following irradiation to 1.25×10^{11} p/cm², a pronounced softening of the knee was

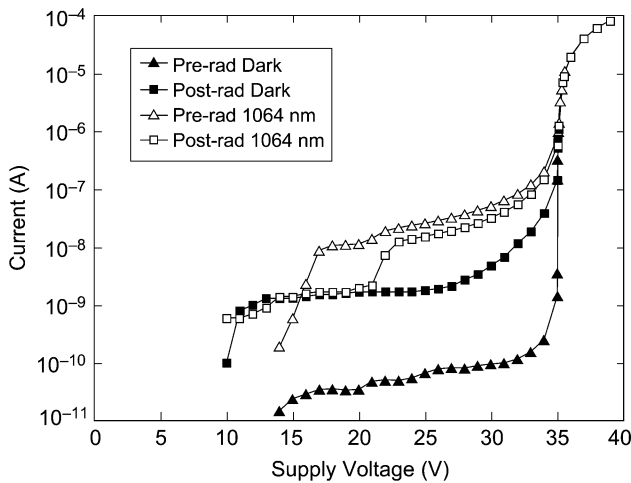


Fig. 8. Pre- and post-irradiation IV curves for Spectrolab sample #1 at 200 K.

observed, along with decreased photocurrent values above the punch through voltage (~ 20 V). We attribute the softening of the dark IV curve to the effect of displacement-damage-induced generation centers created during the proton irradiation; generation centers are sources of thermal dark current. Dark current values were one to two orders of magnitude higher at all supply voltage levels following irradiation, making the onset of Geiger mode less abrupt, and the knee of the IV curve less sharp. Similarly, the creation of displacement-damage-induced *recombination* centers is the expected cause of the reduction in photocurrent values following irradiation. Given these combined effects, there is a much smaller difference between the dark current and photocurrent values at supply voltages near the breakdown voltage, which is consistent with the reduced counting efficiency that was observed at this fluence.

Sample #2, irradiated to only 3.1×10^{10} p/cm², showed similar degradation in counting efficiency at 200 K. However, photon counting was observed when the temperature was dropped to 100 K. Figs. 9 and 10 compare pre- and post-irradiation count rates (using 1534 nm photon illumination) for sample #2 at 200 K and 100 K, respectively.

IV. SUMMARY

We have performed radiation experiments on two emerging high gain, low noise detectors. Our results indicate that these technologies would be fairly sensitive to radiation effects in a space-born application, but there is room for additional radiation characterization. The worst case operational condition during irradiation could be evaluated for the IDA technology, and testing could be performed to lower cumulative levels of DDD and TID than explored here, in order to bound performance degradation from dose effects.

Silicon internal discrete avalanche photodiodes experienced significant mode shifts after irradiation to 5 krad(Si). Future radiation testing of the IDA technology could be performed with test samples irradiated in an unbiased mode, to see if this lessens the impact on device functionality. The biased irradiations used in our study may represent the worst case for this technology, as

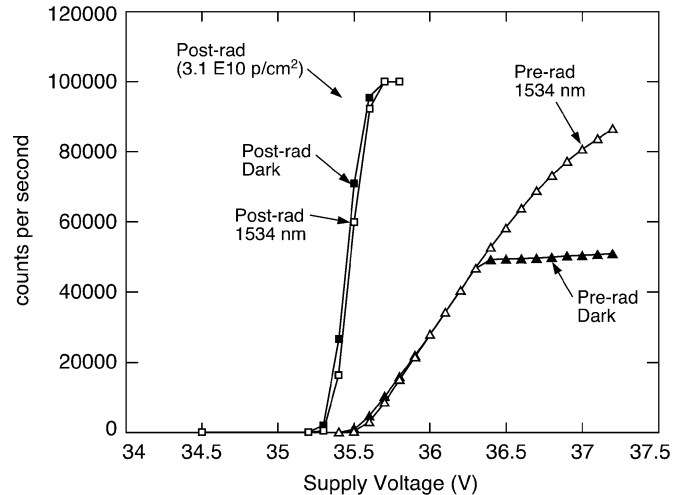


Fig. 9. Pre- and post-irradiation count rates for Spectrolab sample #2 at 200 K (1534 nm).

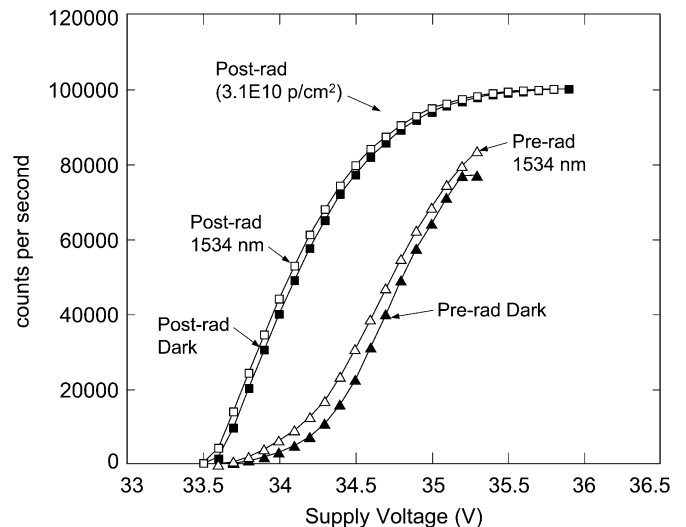


Fig. 10. Pre- and post-irradiation count rates for Spectrolab sample #2 at 100 K (1534 nm).

is often the case for CMOS devices. Recovery may be improved by performing biased anneals at room temperature, high temperature anneals, or by changing the operational temperature to see how the post-irradiation modes of operation are affected. It is also possible that other implementations of the IDA concept may be inherently more radiation tolerant.

InGaAs/InAlAs APDs showed large reductions in detection efficiency after 51-MeV proton fluences of 3.1×10^{10} p/cm² or more (although improved efficiency was observed by reducing the temperature to 100 K). The reduced detection efficiency and softening of the IV curves can be attributed to an increased number of radiation-induced generation and recombination centers following proton irradiation.

ACKNOWLEDGMENT

The authors would like to thank Ronald Ruiz of the Jet Propulsion Laboratory for focused ion beam etching and scanning electron microscope analysis of the IDA technology.

REFERENCES

- [1] P. P. Webb, R. J. McIntyre, and J. Conradi, "Properties of avalanche photodiodes," *RCA Rev.*, vol. 35, pp. 234–278, Jun. 1974.
- [2] R. J. McIntyre, "The distribution of gains in uniformly multiplying avalanche photodiodes: Theory," *IEEE Trans. Electron Devices*, vol. 19, no. 6, pp. 703–713, Jun. 1972.
- [3] V. Shubin and D. Shushakov, "Multi-element avalanche photosensor," *Proc. SPIE*, vol. 2415, pp. 94–103, 1995.
- [4] A. V. Krutov, E. E. Godik, and W. Seemungal, "Highly sensitive silicon photodetectors with internal discrete amplification," *Proc. SPIE*, vol. 5353, pp. 29–35, 2004.
- [5] D. A. Shushakov and V. E. Shubin, "High sensitivity, high resolution detection of signals," U.S. Patent 6,885,827, Apr. 26, 2005 [Online]. Available: <http://www.uspto.gov>
- [6] N. Li, "InGaAs/InAlAs avalanche photodiode with undepleted absorber," *Appl. Phys. Lett.*, vol. 82, no. 13, pp. 2175–2177, Mar. 31, 2003.
- [7] M. A. Krainak, Photon Counting Detectors for the 1.0-2.0 Micron Wavelength Range, Apr. 29, 2005 [Online]. Available: <http://esto.nasa.gov/conferences/estc2004/papers/b3p1.pdf>
- [8] H. N. Becker and A. H. Johnston, "Dark current degradation of near infrared avalanche photodiodes from proton irradiation," *IEEE Trans. Nucl. Sci.*, vol. 51, no. 6, pp. 3572–3578, Dec. 2004.